Digest Journal of Nanomaterials and Biostructures Vol. 19, No. 4, October-December 2024, p. 1921-1935

Synthesis of HMDSO/TiO_2 composite on quartz crystal microbalance for enhanced volatile organic compounds gas sensing properties

L. Grine [a,*], A. Bellel [a], K. Dallah [a], S. Sahli [b]
[a] *Laboratory of Study of Electronic Materials for Medical Applications (LEMEA-MED), University of Frères Mentouri Constantine 1, Constantine 25000, Algeria*
[b] *Laboratory of Microsystems and Instrumentations (LMI), University of Frères Mentouri Constantine 1, Constantine 25000, Algeria*

In this study, HMDSO/TiO_2 nanocomposite was synthesized on a quartz crystal microbalance (QCM) transducer by atmospheric pressure plasma jet (APPJ) for the detection of volatile organic compounds (VOCs). Fourier-transform infrared spectroscopy (FTIR) analysis revealed the presence of Ti-O-Ti bond around 580 cm^{-1}, indicating the growth of TiO_2 film on the HMDSO support layer. X-ray diffraction (XRD) analysis confirmed the presence of rutile and anatase phases of TiO_2, demonstrating that the APPJ method can produce crystalline films in a single process without post-thermal annealing. Atomic force microscopy (AFM) imaging showed the growth of rougher surface QCM coating, leading to an increased specific surface area and more absorption sites. Water contact angle (WCA) measurements showed that the hydrophilic QCM surface was transformed into super-hydrophobic one after coating with the HMDSO/TiO_2 hybrid film. Compared to single layer VOCs sensors, the HMDSO/TiO_2 heterostructure revealed good sensitivity, low response and recovery times across the explored VOC concentration range.

(Received September 26, 2024; Accepted December 9, 2024)

Keywords: Quartz crystal microbalance, Heterostructure, Chemical sensor, Volatile organic compounds, Atmospheric pressure plasma jet

1. Introduction

With the increasing development of industrial technology, considerable quantities of harmful gases such as organic volatile compounds (VOCs) are released into the atmosphere, causing severe environmental problems and human diseases [1, 2]. VOCs pollutants vary in their chemical and electrical properties and safe concentration limits and are often found in gas mixture [3]. Consequently, major environmental and health agencies globally have set rigorous exposure guidelines to mitigate the adverse health impacts of VOCs even at minimal concentrations [4]. Monitoring the levels of pollutant gas concentration is a critical task in various sectors, including industrial safety, environmental protection and public health [5]. In this context, chemical sensors which can detect different chemical molecules are beneficial for addressing these environmental hazards. Recent technologies permitting the development of cost-effective, highly sensitive and compact chemical sensors, capable to detect VOCs vapors in environment have motivated significant interest in scientific research, particularly for applications related to health [6]. Among the various sensor technologies, the quartz crystal microbalance (QCM) stands out for its exceptional sensitivity in gas detection, straight forward experimental configuration, cost-effectiveness and ability in real-time detection of target molecules [7]. QCM is a flexible platform for quick analysis of substances in both liquid and gas phases through the detection of QCM oscillation frequency changes caused by the adsorption of target molecules [8]. Given their operation at room temperature and digital frequency output, QCM transductions are gaining importance in gas sensing applications. The sensing properties of QCM based sensors is based on the physicochemical properties of the sensing layer, emphasizing the importance of material selection in sensor design. Metal oxide nanomaterials such as ZnO [9], WO_3 [10], SnO_2 [11] and TiO_2 [12], are particularly accommodate for sensing

* Corresponding author: Leila.grine@doc.umc.edu.dz
https://doi.org/10.15251/DJNB.2024.194.1921

applications due to their chemical and physical stability and large surface to volume ratio. Titanium dioxide (TiO_2) as a wide-gap semiconductor, has attracted considerable interest in different applications domains like photovoltaic, photocatalysis and chemical sensors [13, 14]. TiO_2's effectiveness in detecting VOCs can be attributed to its large specific surface area, stability and adaptable electronic properties. However, a significant limitation of sensors based on pristine metal oxides like TiO_2 is their need for high operational temperatures (200-350 °C) to enable chemical adsorption and desorption processes, which leads to substantial power consumption and limits their broader application [15]. To address these challenges, recent research has focused on developing sensors that operate at ambient temperatures, thereby reducing energy consumption and enhancing practical utility.

The elaboration of TiO_2 thin layers can be achieved by various methods including magnetron sputtering, plasma-enhanced chemical vapor deposition (PECVD), physical vapor deposition (PVD), chemical vapor deposition (CVD) and the sol-gel process [16-19]. The plasma technique, in particular, offers advantages due to the continuous application of an electric field, which facilitates the dissociation of precursor gases into reactive radicals/ions. These radicals/ions then migrate towards substrates, leading to the formation of the thin film structure [20, 21]. Plasma technologies hold potential advantages over traditional chemical methods by allowing adjustment in process parameters, which can significantly influence the characteristics and performance of the resulting films [20]. The atmospheric pressure plasma jet (APPJ) technique has attracted significant consideration within the scientific community for its lower maintenance needs, reduced functioning costs and the avoidance of vacuum systems [22]. APPJ was considered as an efficient means to produce plasma plumes with high ionization level of excited species [22, 23]. Thereby, APPJ has been applied across various fields including the synthesis of bio-materials, polymers, nanoparticles and thin film deposition [24-26]. Particularly, the APPJ method has makes possible the production of crystalline thin films in an individual step, eliminating the necessity for post-annealing treatments [27]. The generation of plasma through APPJ requires energizing a gas to alter the atoms and molecules electronic structures, thereby creating excited species. This energy may be derived from thermal sources, electric currents or electromagnetic radiation [28]. Among the three different phases of TiO_2 films (anatase, rutile and amorphous), anatase phase TiO_2 films have better sensitivity to volatile organic compound gases than rutile and amorphous phases [29]. In plasma process, TiO_2 anatase phase can be directly synthesized through substrate heating during deposition [30], application of substrate bias voltage [31] or through post-deposition annealing [32]. Furthermore, in VOCs sensing applications, the design of TiO_2 layers with highly hydrophobic surface characteristics enhance the operational stability against the interference of high humidity which may originate from ambient conditions [33]. The Hydrophobic surface of TiO_2-based sensor can effectively prevent the adsorption of water vapor during the VOCs detection [33]. However, challenges such as poor adhesion between the TiO_2 and the QCM gold electrode can impact sensor performance and reliability, often attributed to the surface roughness or the quality of the coating [34, 35]. To deal with this issue, employing intermediate layer or utilizing surface modification techniques can significantly improve adhesion [36, 37]. On this basis, this work aims to explore a cost-efficient solution of using hexamethyldisiloxane (HMDSO) and TiO_2 heterostructure to enhance adhesion and exploit the complementary advantages of both materials, resulting in improved sensitivity and reliability for VOCs monitoring. Many research studies have shown that fabricating heterostructures has emerged as a straight forward and effective approach to improve sensing properties [38]. As an example, S. Jayawardena et al. produced a QCM gas sensor coated with GO/TiO_2 heterostructure [39]. They have shown that despite single TiO_2 layer has no stronger gas sensing capacity, the elaboration of the composite significantly improves the sensor sensitivity by increasing the gas adsorption sites quantity and sensor specific surface area. Similarly, K. Tang et al. successfully synthesized GO/MoS_2 nanocomposite on QCM transducer by hydrothermal technique for relative humidity sensing [40]. They have found that GO/MoS_2-based sensor exhibited three times the sensitivity obtained on pure GO sensor. These investigations demonstrated that heterostructures enable effective improvements in the gas sensing properties.

The present study reports gas sensing characteristics of HMDSO/TiO_2 composite coated QCM transducer. The organosilicon thin layer was initially deposited on QCM gold electrode through a simple plasma jet technique from pure vapor of HMDSO. Subsequently, TiO_2 thin film

was synthesized over the functionalized QCM surface using a plasma jet system from a mixture of oxygen and titanium isopropoxide (TTIP) to form a stable HMDSO/TiO_2 hybrid film. As far as we know, the preparation of HMDSO/TiO_2 composite on QCM transducer for VOCs sensing application has not yet been investigated. The chemical structures of the elaborated films and their corresponding morphologies are characterized using, X-ray diffraction (XRD), Fourier-transformed infrared spectroscopy (FTIR) and atomic force microscopy (AFM), respectively. The hydrophobicity property of the QCM coating was assessed by contact angle measurements. The HMDSO/TiO_2 based sensor responses have been evaluated at room temperature towards different concentrations of benzene, methanol, ethanol and toluene ranging from 17 to 70 ppm. The selected VOCs are known for their environmental hazards [41]. The study established that the HMDSO/TiO_2 nanocomposite exhibits enhanced sensing performance, with rapid response/recovery times and a low detection limit, suggesting its potential for real-time monitoring of VOCs pollutants.

2. Experimental

2.1. Elaboration of HMDSO/TiO_2 hybrid film using APPJ

Both films deposition has been carried out using atmospheric pressure plasma jet consisting of high voltage (HV) and grounded electrodes centered around quartz tube (Figure 1). The HV electrode is powered with radio frequency generator (13.56 MHz). The APPJ deposition technique generally utilizes a monomer carried by an inert gas which is mixed with a feed gas before passing through the plasma discharge region. In this zone, plasma reactive species are produced from the mixture of precursor and feed gas, then transferred to substrate surface for film deposition [41]. In this work, thin HMDSO film was deposited using hexamethyldisiloxane (C6H18OSi2, HMDSO, 98%, Sigma Aldrich Ltd) as the organosilicon precursor. Argon has been used for plasma discharge generation and to transport the precursor vapor to the glow discharge zone. Argon with a flow rate of 5 slm was bubbled through HMDSO to produce saturated monomer vapor with a flow rate of 0.18 slm. During deposition, the argon flow rate was maintained at 5 slm and introduced from the top of the APPJ system to create the plasma jet. The typical Ar/HMDSO APPJ operated by a 120 W radio frequency (13.56 MHz) power supply is shown in Figure 1. The distance between the substrate and the plasma jet was set to 24 mm to prevent powder formation and to avoid substrate thermal damage. During deposition, substrates were moved beneath the discharge area using an xy-linear system at a velocity of 21 mm/s to ensure uniform coating. All films depositions were performed on AT-cut quartz crystals with a fundamental oscillation frequency of 5 MHz and circular gold electrode of 8 mm diameter and crystalline (100)-oriented silicon substrates. Prior to deposition, substrates were cleaned with acetone, rinsed in distilled water and then dried in air. In case of titanium dioxide deposition, titanium (IV) isopropoxide (Ti $[OCH(CH_3)_2]_4$, TTIP, 99.999%, Sigma Aldrich Ltd.) was used as the organometallic precursor. The monomer solution was maintained in a heated container equipped with a magnetic stirrer and the precursor vapor was generated through an argon bubbling system (Figure 1). The saturated monomer vapor is then transported close to the plasma nozzle outlet generated by argon. The argon flow rate and plasma power were maintained at 2 slm and 50 W (13.56 MHz), respectively. Oxygen necessary for forming titania films was supplied from atmosphere.

In this study, the plasma organosilicon layer was employed as a substrate for the growth of TiO_2 particles to achieve well-adherent crystalline thin TiO_2 film and enhance the performance of the hybrid layer as a chemical sensor. Previous researches on the deposition of TiO_2 films by APPJ from TTIP precursor, using argon as both working and carrier gas with nearly similar flow rates, have demonstrated the growth of homogeneous columnar films predominantly crystallized in the anatase phase [41, 42]. The film thicknesses of HMDSO and HMDSO/TiO_2, measured using a Tencor profilometer, were approximately 170 nm and 494 nm, respectively.

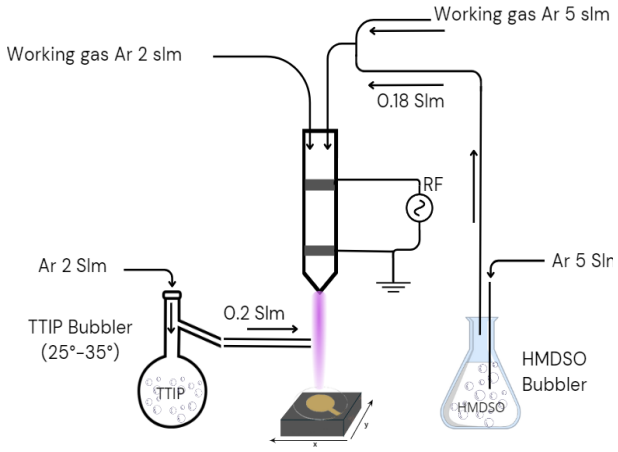

Fig. 1. APPJ Experimental setup for the elaboration of HMDSO and HMDSO/TiO_2 heterostructure.

2.2. Materials characterization

The QCM coating surface wettability was evaluated through WCA measurements, carried out immediately after plasma deposition. Water droplet (5 µl) was deposited on the QCM coated surface by a micro syringe, then the droplet's image was captured using a numerical camera and transmitted to a computer for contact angle estimation. To investigate the crystallographic properties of the QCM coatings, X-ray diffraction (XRD) analysis was performed (ARL EQUINOX 100 X-ray diffractometer) using Cu-Kα radiation source. This analysis offers information concerning the crystal orientations and materials phase composition, which are critical for understanding the structural characteristics that influence the sensor's performance. Chemical bonding structures within the film were examined by Fourier Transform Infrared spectroscopy (FTIR) analysis. FTIR spectra were recorded in the absorption mode (500 to 4000 cm^{-1}) using a JASCO FT/IR-6300 type A spectrometer. This technique is essential for identifying functional groups and chemical bonds within the hybrid film, offering a molecular-level view of the composite material. The surface morphology of the elaborated layers was analyzed using AA2000 (Angstrom Advanced Inc USA) atomic force microscope (AFM). Measurements were taken at room temperature in tapping mode, which helps to minimize tip-sample interactions and provides high-resolution topographical imaging. The associated AFM software was utilized to calculate the average surface roughness, further elucidating the textural characteristics of the film which are crucial for enhancing the sensor's adsorptive properties.

2.3. HMDSO/TiO_2 sensing properties evaluation

The operating principal of the QCM sensor relies on the detection of the frequency shift (Δf) resulting from the adsorption of analyte molecules from the gas phase. The frequency shift are directly correlated to the change in oscillating mass (Δm) by the Sauerbrey equation [43] given by:

$$\Delta f = -\frac{C_f f_0^2}{A} \Delta m \quad (1)$$

where C_f is the mass sensitivity constant of the quartz crystal (2.26×10^{10} $m^2 s\ g^{-1}$), A is the sensitive layer area and f_0 is the quartz crystal fundamental resonance frequency (5 MHz). The sensor response measurements were conducted inside a custom-built chamber equipped with precise controls of temperature and relative humidity. Figure 2 shows the schematic of the testing system where the QCM sensor is connected to the gas sensing setup for recording the Δf as a function of time in absorption and desorption mode. The sensitivity of the elaborated QCM sensors were evaluated towards different concentration of VOCs molecules. A liquid of organic compound was injected into the measurement chamber and heated until evaporation. The concentration of the introduced VOCs vapor was calculated in parts per million (ppm) using the following equation [44].

$$C = \frac{22.4\rho TV_S \times 10^3}{273MV} \quad (2)$$

where C is the analyte concentration in ppm, ρ is the density of the liquid analyte in g/ml, V_s is the liquid volume in µl, M is the molecular weight of the analyte in g/mol, T is the temperature inside the testing chamber in °K and V is the testing cell volume in L. During the experiments, frequency shifts were meticulously recorded using a QCM200 digital frequency counter from Stanford Research Systems (USA) and data were stored in personal computer through LabVIEW software. The HMDSO/TiO_2 coated QCM sensors underwent testing with low concentrations of benzene, toluene, ethanol and methanol (17 to 70 ppm) which are selected for their importance in environmental and industrial safety. Upon stabilization of the frequency shift, indicating equilibrium absorption of VOCs, the sensor was purged with dry air to desorb the analytes and restore baseline frequency, a critical step for assessing recovery capability and readiness for subsequent measurements.

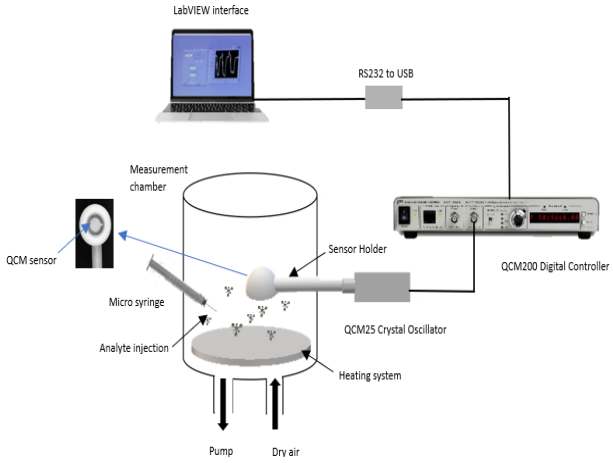

Fig. 2. Layout of the measurement chamber.

3. Results and discussion

3.1. Hydrophobicity of elaborated thin layers

In this work, the surface wettability of elaborated QCM coating was evaluated by WCA measurements. The HMDSO film deposited on QCM substrate using a 120 W powered APPJ, possesses a WCA of approximately 140°, indicating a highly hydrophobic nature of the deposited layer (Figure 2). Y. Lin et al. have reported nearly the same value of water contact angle (143°) measured on surface of HMDSO film elaborated by atmospheric pressure plasma jet [45]. Previous research suggests that the hydrophobic characteristics of HMDSO surfaces are attributed to the presence of methyl (–CH_3) functional groups within the film's structure [46]. The topography of the deposited films is also an important factor affecting surface wettability. By applying a thin TiO_2 layer via plasma jet onto the pre-deposited HMDSO film, the surface retains its hydrophobic properties. The resulting HMDSO/TiO_2 hybrid layer exhibited a WCA greater than 130° (Figure 3). This water-repellent feature in VOCs detection application provides the sensor with good stability in both relatively dry and ultra humid atmospheres.

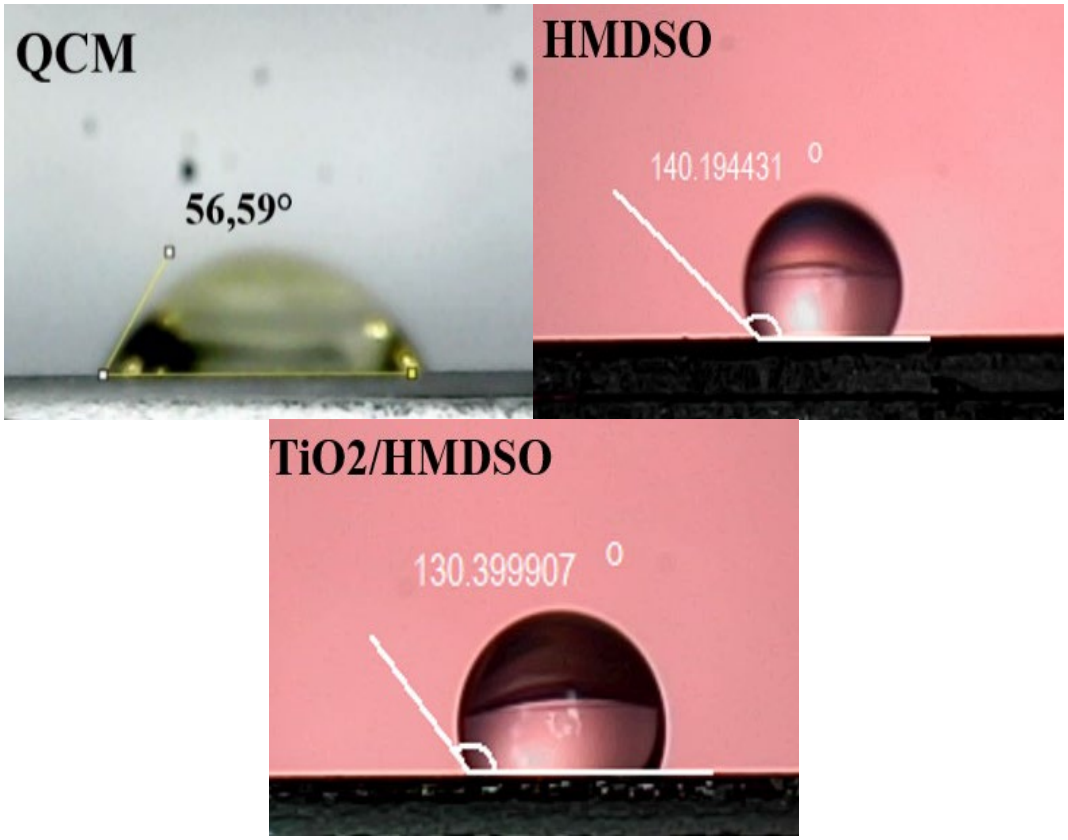

Fig. 3. Water contact angle Measurements on: QCM electrode, HMDSO and HMDSO/TiO_2 surfaces.

3.2. Film characterization

To elucidate the impact of the chemical structure on the sensing behaviors of the deposited QCM coatings, FTIR analyses were carried out. Figure 4 displays the FTIR spectra for both HMDSO/TiO_2 composite and the pristine HMDSO, recorded in the 500-4000 cm-1 wavenumber range. The FTIR spectrum related to the HMDSO film shows the presence of a distinctive peak corresponding to the Si–O–Si absorption band. The peaks located at 800 cm^{-1} and 1014 cm^{-1} are assigned to the Si–O–Si bending vibration and asymmetric stretching, respectively [47-49]. The peak around 2931 cm^{-1} is associated with CH_x stretching vibrations, mainly corresponding to the asymmetric stretching of methyl groups (CH_3). Additionally, a wide peak around 3409 cm^{-1} corresponding to hydroxyl groups is commonly attributed to water molecules adsorbed on the coating surface. The chemical structure of the TiO_2 coated HMDSO surface, analyzed by FTIR technique is depicted in Figure 4. The FTIR spectrum of the HMDSO/TiO_2 heterostructure was rather different from that of HMDSO film alone. The clear difference was in the existence of Ti-O stretching peak around 580 cm^{-1}, demonstrating the deposition of TiO_2 film on the HMDSO layer [50]. The detection of sharp peak near 580 cm^{-1} instead of wide band (800-400 cm^{-1}) reveals that APPJ deposition technique was efficient to develop the crystalline structure of TiO_2 films without the need for an annealing process [51-53]. Furthermore, the HMDSO/TiO_2 spectrum exhibited additional vibrational signatures, including an absorption associated with the C=C bond near 1627 cm^{-1} and a peak indicative of C=O stretching vibrations at 2343 cm^{-1}. The OH broad peak located around 3200 cm^{-1} and 3500 cm^{-1} is also noticed, which may be attributed to adsorbed moisture.

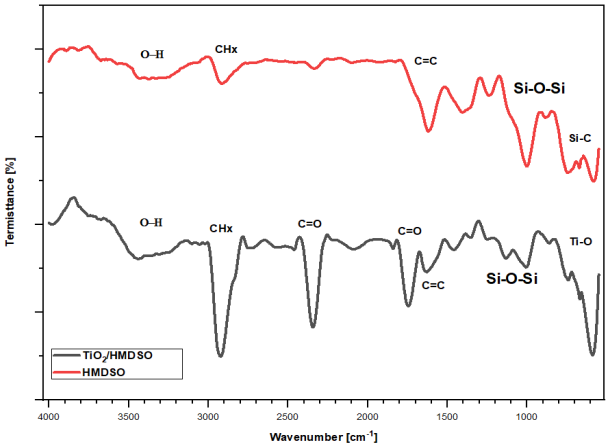

Fig. 4. FTIR spectra of HMDSO and HMDSO/TiO_2 heterostructure.

The crystalline structure of the elaborated HMDSO/TiO_2 composite has been evaluated by X-ray diffraction analysis. XRD patterns presented in Figure 5 revealed the presence of multiple phases of titanium dioxide at 2θ≈29.2°, 38.2°, 44.2° and 56.4° suggesting the presence of the anatase phase, that corresponds to (101), (112), (004) and (200) diffraction planes of anatase, respectively [54]. Even though the most noticeable phase is anatase, XRD patterns also revealed the presence of rutile phase. Peak at 2θ≈ 42.2°, 47.8° and 64.1° matches the rutile phase of TiO_2, corresponding to the (101), (111) and (211) diffraction planes of rutile, respectively [54]. The presence of organosilicon layer in the composite sample does not produce a distinct peak in the XRD patterns, suggesting that the organic layer might be present in an amorphous form [55]. The sharpness and intensity of the observed XRD peaks indicates a good degree of crystallinity in the metal oxide film, reflecting well-ordered crystal structure. Throughout the elaboration of TiO_2 layer, the TTIP monomer was directly introduced into the plasma discharge aera, where gas phase reactions and the resulting development of crystalline TiO_2 nanoparticles are assisted by high excited species density and the relatively high gas temperature [56]. Regarding the correlation between sensing properties and film crystallinity, some research works have reported that the increased crystallinity of TiO_2 nanoparticles enhances their gas-sensing capabilities [51].

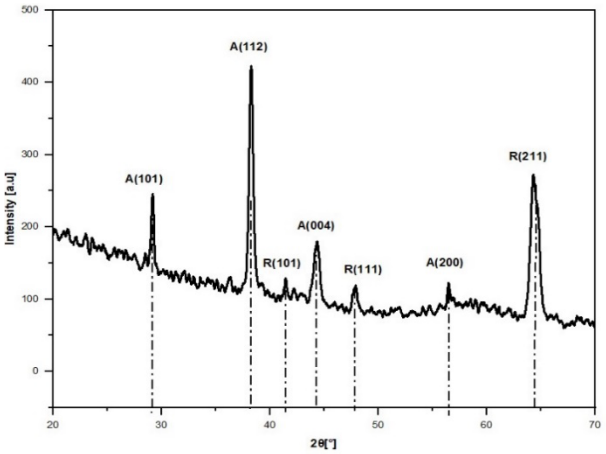

Fig. 5. XRD patterns of the investigated HMDSO/TiO_2 heterostructure.

The average crystalline size was calculated using the full width at half maximum (FWHM) of the most intense peak by the Debye-Scherrer formula given by:

$$D = \frac{0.89\lambda}{(\beta \cos \theta)}$$

where, D represents the average crystalline size, λ is the wavelength of X-ray radiation (Cu Kα, 0.15406 nm), β in radians is the FWHM of the XRD peak and θ is the diffraction angle [57]. The TiO_2 average particle size was evaluated to be approximately 16 nm. Notably, a smaller particles size corresponds to a large specific surface area and more absorption sites leading to the improvement of sensor sensitivity.

3.3. Surface morphology analysis

Surface morphology is assumed to affect significantly the sensing capability of the studied hybrid layer. The AFM images recorded in tapping mode are presented in Figure 6a and Figure 6b for HMDSO film and HMDSO/TiO_2 composite, respectively. The particles aggregate of HMDSO give rise to relatively uniform sea-island structure (figure 6a). The higher surface features around 68 nm as illustrated by the z scale indicates that HMDSO film elaborated by APPJ exhibited rougher surface with root mean square roughness of about 13.6 nm. HMDSO layer which acts as a support for TiO_2 film is expected to accommodate a great specific surface area for the growth of titanium oxide particles. Upon deposition of about 324 nm thick TiO_2 layer by RF APPJ, the initial substrate roughness of 13.6 nm increased to about 61 nm by the agglomeration of TiO_2 nanoparticles (Figure 6b). The AFM image illustrates the growth of a columnar structure with voids appearing between the columns. D. Li et al observed a similar topography for TiO_2 film deposited by PECVD [58]. They have reported that for thin film, AFM image showed the development of thin columns making the surface not so rough. With increasing film thickness, the size of column got larger and a quantity of voids are promoted due to columns separation, as a result, the surface becomes rougher. This increased roughness and the resulting higher surface to volume ratio enhance the sensor's adsorptive properties. The columnar and porous nature of the TiO_2 structure not only provides more surface area but also facilitates the diffusion of target VOCs molecules through its pores and void regions. This capability is particularly valuable for mass sensing applications, where the penetration of VOCs molecules into these pores can alter the coated QCM oscillation frequency, enabling sensitive detection even at low analyte concentrations.

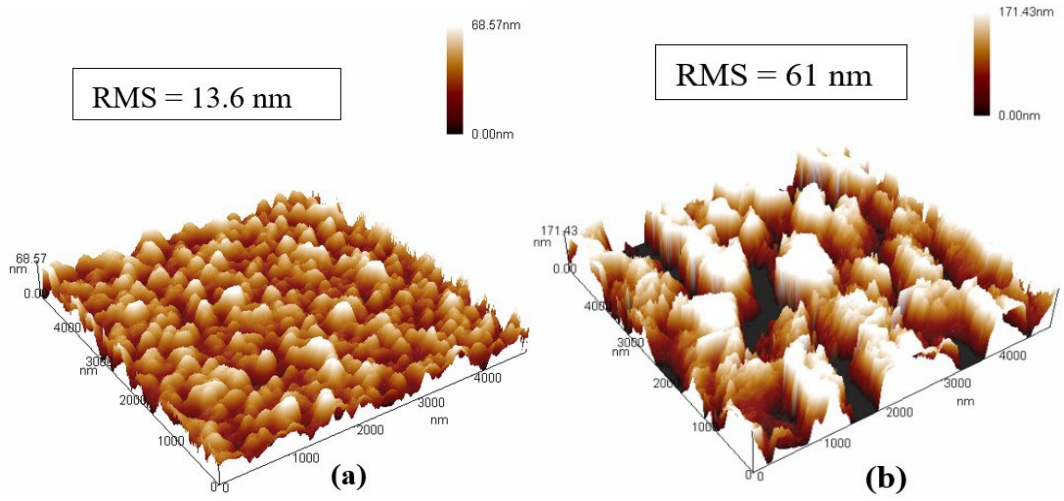

Fig. 6. AFM image of: (a) HMDSO and (b) HMDSO/TiO_2 heterostructure coated QCM.

3.4. Evaluation of sensor response

The initial experiments assessing the sensing performance of HMDSO and HMDSO/TiO_2 composite-functionalized QCM resonators involved their exposure to 70 ppm of toluene, ethanol, benzene, and methanol vapors, followed by dry air as a reference gas. All sensing measurements

were conducted at ambient temperature with a relative humidity of about 40%. For both coated QCM sensor, the shift frequency Δf gradually rises with time and rapidly reached a saturation (figure 7). Upon exposure to dry air, the sensors exhibited a complete reversible recovery of the baseline frequency, indicating effective desorption of the target molecules. Real-time response comparisons, illustrated in Figure 7, reveal that the HMDSO/TiO_2 composite exhibits superior sensing properties compared to the HMDSO film alone. This enhancement is consistent with numerous studies indicating that the combination of TiO_2 with other materials, particularly carbon-based materials, significantly improves the gas sensing devices sensitivity [59-61]. S. Jayawardena et al. [51] specifically noted the advantageous sensing properties of GO/TiO_2 composite. They reported that despite TiO_2 alone demonstrated limited gas adsorption capabilities, the modification of GO with TiO_2 in the composite preparation created numerous interfaces. These interfaces facilitate charge transfer, making the surface more active and increasing the availability of surface-active sites. In this work, the organosilicon layer acting as a support for the growth of TiO_2 film aids to achieve a considerable surface area and an appropriate porous structure as demonstrated by AFM analysis. Consequently, supplementary analyte molecules can be adsorbed due to the increased number of gas adsorption sites and the enhanced surface area. Additionally, the increased crystallinity of TiO_2 nanoparticles, as demonstrated by some researchers, is favorable for gas sensing applications [51]. This is supported by the XRD results, which indicate the growth of both anatase and rutile phases of TiO_2, aligning with the observed improvement in sensor performance. The combined effect of the HMDSO/TiO_2 composite's enhanced surface area, increased number of active sites and improved crystallinity highlight its potential as an effective material for VOCs detection.

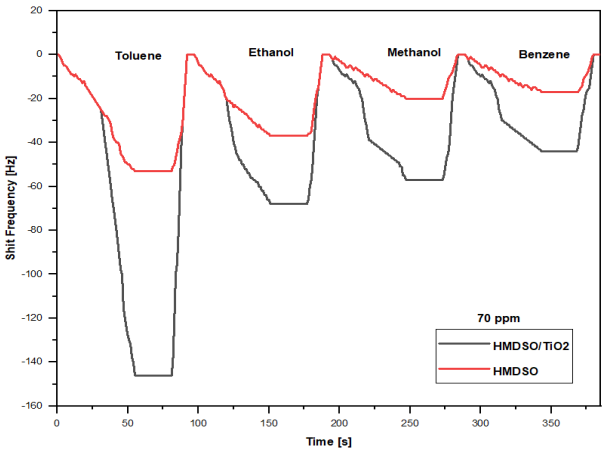

Fig. 7. Dynamic responses of HMDSO and HMDSO/TiO_2 to 70 ppm of toluene, ethanol, benzene and methanol.

Figure 8 a and b depict the typical response and recovery behavior of HMDSO and HMDSO/TiO_2 coated QCM sensor, respectively, when exposed to different concentration of toluene, ethanol, benzene and methanol (17-70 ppm), followed by a purge with dry air. The ability of these sensors to restore to their initial oscillation frequency values after exposure to dry air indicates the full desorption of analytes. For all tested VOCs molecules, the sensor kinetic response indicated that the QCM frequency shift gradually increases as a function of time before attaining a steady state. The sensor achieved equilibrium when the adsorption and desorption processes occurred simultaneously [62]. It is clearly noticed that the TiO_2 film with HMDSO as a support layer (Figure 8b) has a greater response towards all investigated VOCs molecules than the sensor based on pure HMDSO (Figure 8a). Obviously, compared with pure HMDSO film, HMDSO/TiO_2 composite has larger diffusion space for VOCs analytes giving more surface-active sites for sensitivity enhancement. The results indicated that the coated QCM-based sensor had strong affinity towards toluene vapors and the sensitivity decreases with the following sequence: toluene > ethanol >

methanol > benzene. The sensor's affinity for toluene results from several interconnected factors, including molar mass, molecular volume, polarization and specific adsorption sites [63]. Toluene (C_7H_8) has a higher molar mass (92.14 g/mol) than ethanol (C_2H_6O, 46.068 g/mol), methanol (CH_3OH, 32.041 g/mol) and benzene (C_6H_6, 78.11 g/mol) [15], leading to stronger interactions with the HMDSO/TiO_2 sensor surface, thus promoting adsorption and detection. As an apolar compound, toluene exhibits stronger Van der Waals interactions with the sensor surface than the dipolar or π-π interactions present with ethanol, methanol and benzene [64]. Furthermore, the HMDSO/TiO_2 surface presents specific adsorption sites for aromatic molecules [63], facilating the interaction and detection of toluene. In case of smaller molecules (ethanol and methanol), the material sensing mechanism can be explained by adsorption and diffusion processes through the polymeric film pores [65]. However, for benzene, that is relatively larger molecule than ethanol and methanol, the gas sensing mechanism can be restricted to surface adsorption effect only, which explain the weak affinity of the studied sensor towards benzene.

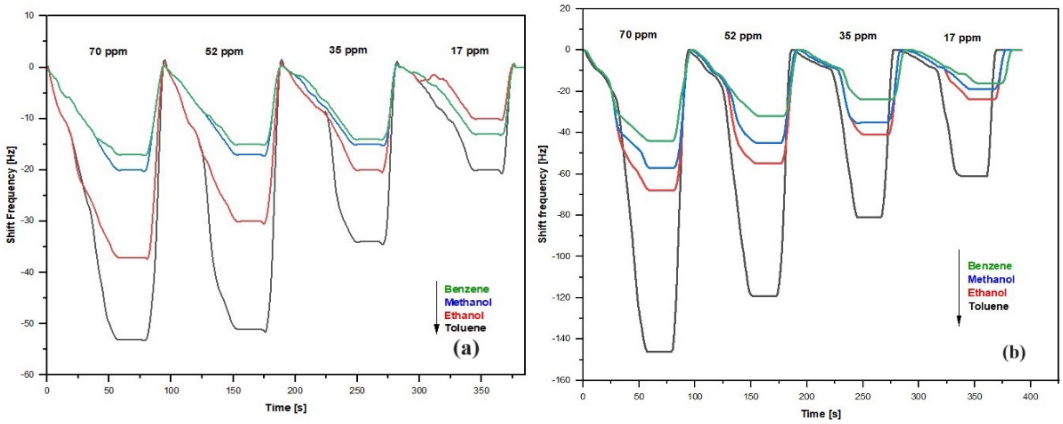

Fig. 8. The real-time frequency responses of QCM sensors coated with: (a) HMDSO and (b) HMDSO/TiO2 towards various VOCs concentrations.

Calibration curves plotted using saturation values of Δf as a function of VOCs concentration are shown in Figure 9. It is evident that all sensor responses in the studied VOCs range present a satisfactory linear relationship with VOCs concentration, describing by equation y = 0.32x-36.27, with a linear fit of $R^2 = 0.989$.

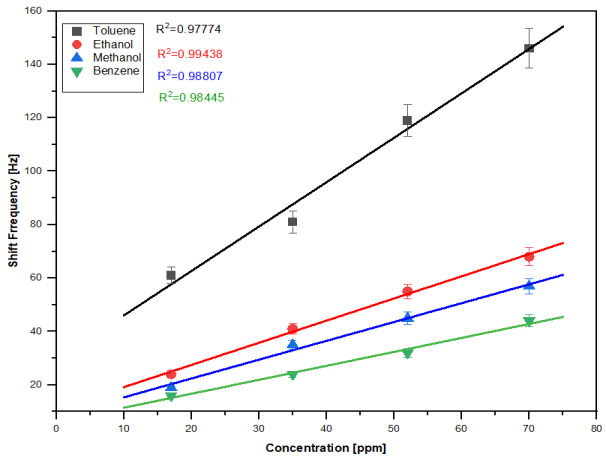

Fig. 9. Calibration curves for maximum sensitivity of the HMDSO/TiO_2 coated QCM sensor.

The sensor sensitivity (S) was extracted from the calibration curve slope and the limit of detection (LOD) is determined by the relation 3σ/S, where S is the sensor sensitivity towards particular VOC molecule and σ is the noise standard deviation [66]. Throughout the experiments, the QCM controller shows only minor fluctuations (±1 Hz), thus setting the noise level at 1 Hz for the sensor. The values of S and LOD for HMDSO and HMDSO/TiO_2 composite coated QCM sensors are summarized in Table 1. The sensitivity comparison between HMDSO/TiO_2 composite and pure HMDSO for VOCs sensing clearly demonstrates that the heterostructure exhibits significantly higher sensitivity. This increase is attributed to the synergistic effects of combining the excellent properties of each material, resulting in enhanced performance for VOC detection. Similar enhancements in sensitivity through the use of composite materials have been reported by S. Jayawardena et al. [51] in the development of a graphene oxide/TiO_2 composite and by D. Zhang et al. [67] in the conception of a humidity sensor based on a Metal Oxide/Graphene hybrid nanocomposite. In addition, the LOD of the composite developed in this study was about 2 and 5 better in case of toluene and benzene sensing, respectively (Table1).

Table 1. Sensing properties of the investigated sensor.

	HMDSO		HMDSO/TiO_2	
VOCs	Sensitivity [Hz/ppm]	LOD [ppm]	Sensitivity [Hz/ppm]	LOD [ppm]
Toluene	0.66	4.55	1,66	1.81
Ethanol	0.5	7	0.88	3.41
Benzene	0.12	25	0.69	4.35
Methanol	0.1	30	0.53	5.66

The sensors response and recovery speeds are crucial for their practical applications. The response time corresponds to the period required for the QCM sensor to achieve 90% of the maximum frequency shift, while the recovery time corresponds to the period necessary for restoring frequency baseline after purging with dry air. The variations of the response and recovery times as a function of analyte concentration are shown in Figure 10. The sensor rapidly reaches equilibrium, taking approximately 12 seconds in response to a step change in VOCs concentration (70 ppm). Similarly, the recovery time is notably short, approximately 6 seconds at 17 ppm, indicating quick desorption of the target molecules. The faster response/recovery time might be due to the porous structure and suitable film thickness, which facilitate the rapid diffusion of molecules through the sensing layer [40], suggesting that physical absorption plays an important role in the sensing mechanism. However, from Figure 10 it is clearly noticed that response/recovery time increases with increasing analyte concentration because a greater number of target molecules interacts with the sensing layer at higher VOC concentrations.

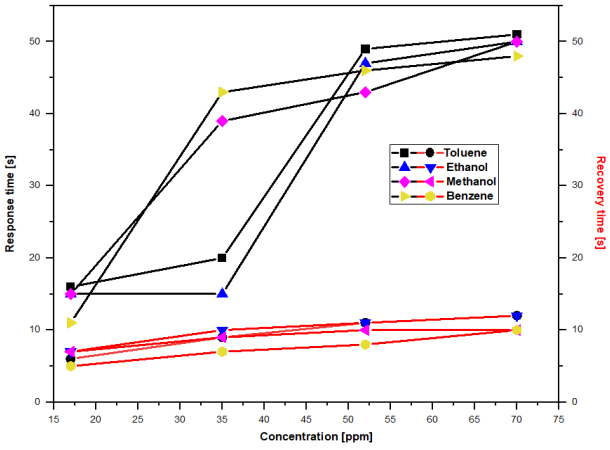

Fig. 10. Response/recovery time of the HMDSO/TiO_2 based sensor as a function of VOCs concentration.

4. Conclusion

In this study, HMDSO/TiO_2 composite has been successfully elaborated by an atmospheric pressure plasma jet technique on QCM transducer for room temperature detection of volatile organic compounds. Initially, an organosilicon thin layer was elaborated on gold QCM electrode by APPJ technique from HMDSO precursor. Subsequently, TiO_2 thin film was grown on the pre-deposited HMDSO layer through a similar synthesis technique with TTIP as precursor. The characteristics data obtained from FTIR and XRD indicated that crystallization of titanium dioxide could be achieved in APPJ without post annealing. Both deposited thin films show rough surfaces as confirmed by high RMS values obtained from AFM measurements, which led to a large specific surface area.

The synergistic interaction between HMDSO and TiO_2 in the composite material resulted in more active sites, significantly enhancing the sensor's performance. The HMDSO/TiO_2 composite sensing properties were analyzed by exposing the developed sensor to various concentrations of toluene, benzene, methanol and ethanol. The sensor showed rapid response and recovery times, high sensitivity, excellent reproducibility and strong affinity towards toluene molecules, able of sensing a low concentration of about 1.81 ppm at a relatively low operating temperature of 24 ºC. The promising sensing performance of the studied hybrid layer suggests its potential for diverse environmental monitoring applications. However, further research is needed to address the challenges of utilizing the HMDSO/TiO_2 composite material in practical applications.

References

[1] E. David, V.-C. Niculescu, International Journal of Environmental Research and Public Health, vol. 18, no. 24, p. 13147, 2021; https://www.mdpi.com/1660-4601/18/24/13147.
[2] X. Zhou, X. Zhou, C. Wang, H. Zhou, Chemosphere, vol. 313, p. 137489, 2023/02/01/ 2023; https://doi.org/10.1016/j.chemosphere.2022.137489.
[3] E. A. Silva, M. L. Braunger, A. Gregori, C. A. Olivati, SN Applied Sciences, vol. 1, no. 3, p. 200, 2019/02/01 2019; https://doi.org/10.1007/s42452-019-0187-z
[4] N. Pinthong, S. Thepanondh, A. Kondo, Aerosol and Air Quality Research, vol. 22, no. 2, p. 210064, 2022; https://doi.org/10.4209/aaqr.210064
[5] C. Lai et al., Coordination Chemistry Reviews, vol. 427, p. 213565, 2021/01/15/ 2021; https://doi.org/10.1016/j.ccr.2020.213565.
[6] Y. Kim, Y. Jeon, M. Na, S.-J. Hwang, Y. Yoon, Sensors, vol. 24, no. 2, p. 431, 2024; https://www.mdpi.com/1424-8220/24/2/431.
[7] N. Alanazi, M. Almutairi, A. Alodhayb, Sens Imag 24 (1): 10, 2023; https://doi.org/10.1007/s11220-023-00413-w
[8] H. Selvi, I. Capan, R. Capan, Y. Acikbas, Journal of Materials Science: Materials in Electronics, vol. 35, no. 18, p. 1268, 2024; https://doi.org/10.1007/s10854-024-13087-1
[9] N. N. Prabhu, B. Shivamurthy, S. Anandhan, R. BV, J. C. RB, Cogent Engineering, vol. 11, no. 1, p. 2403702, 2024; https://doi.org/10.1080/23311916.2024.2403702
[10] S. Ghodrati, Synthesis and Characterization of Polymeric Sensing Materials for Detection of Gases in Energy Storage Devices, University of Waterloo, 2024.
[11] I. Kononova, V. Moshnikov, P. Kononov, Gels, vol. 9, no. 4, p. 283, 2023; https://www.mdpi.com/2310-2861/9/4/283
[12] J. M. Rzaij A. M. Abass, J. Chem. Rev, vol. 2, no. 2, pp. 114-121, 2020; https://doi.org/10.33945/SAMI/JCR.2020.2.4
[13] A. Afzal, A. Habib, I. Ulhasan, M. Shahid, A. Rehman, Frontiers in materials, vol. 8, p. 687059, 2021; https://doi.org/10.3389/fmats.2021.687059

[14] M. Rafique et al., ACS omega, vol. 8, no. 29, pp. 25640-25648, 2023; https://doi.org/10.1021/acsomega.3c00963
[15] A. A. Haidry et al., TrAC Trends in Analytical Chemistry, vol. 170, p. 117454, 2024/01/01/ 2024; https://doi.org/10.1016/j.trac.2023.117454.
[16] B. Astinchap, H. Ghanbaripour, R. Amuzgar, Optik, vol. 222, p. 165384, 2020/11/01/ 2020; https://doi.org/10.1016/j.ijleo.2020.165384.
[17] C. Esparza-Contro et al., Surface and Coatings Technology, vol. 389, p. 125643, 2020/05/15/ 2020; https://doi.org/10.1016/j.surfcoat.2020.125643.
[18] B. Dey et al., Surface and Coatings Technology, vol. 436, p. 128256, 2022/04/25/ 2022; https://doi.org/10.1016/j.surfcoat.2022.128256.
[19] D. Macwan, P. N. Dave, S. Chaturvedi, Journal of materials science, vol. 46, pp. 3669-3686, 2011; https://doi.org/10.1007/s10853-011-5378-y
[20] D. Li, S. Dai, A. Goullet, A. Granier, Nano, vol. 13, no. 10, p. 1850124, 2018; https://doi.org/10.1142/S1793292018501242
[21] A. Borras, J. R. Sanchez-Valencia, R. Widmer, V. J. Rico, A. Justo, A. R. Gonzalez-Elipe, Crystal Growth and Design, vol. 9, no. 6, pp. 2868-2876, 2009; https://doi.org/10.1021/cg9001779
[22] S. H. B. Vinoth Kumar et al., Journal of Carbon Research C, vol. 7, no. 4, p. 71, 2021; https://www.mdpi.com/2311-5629/7/4/71.
[23] S. Matsusaka, Advanced Powder Technology, vol. 30, no. 12, pp. 2851-2858, 2019/12/01/ 2019; https://doi.org/10.1016/j.apt.2019.09.023
[24] M. Laroussi, IEEE transactions on plasma science, vol. 43, no. 3, pp. 703-712, 2015; https://doi.org/10.1109/TPS.2015.2403307
[25] H. J. Jang, E. Y. Jung, T. Parsons, H.-S. Tae, C.-S. Park, Polymers, vol. 13, no. 14, p. 2267, 2021; https://www.mdpi.com/2073-4360/13/14/2267.
[26] M. Narimisa, F. Krčma, Y. Onyshchenko, Z. Kozáková, R. Morent, N. De Geyter, Polymers, vol. 12, no. 2, p. 354, 2020; https://www.mdpi.com/2073-4360/12/2/354.
[27] S. Gosavi et al., Catalysts, vol. 11, no. 1, p. 91, 2021; https://www.mdpi.com/2073-4344/11/1/91.
[28] C. Tendero, C. Tixier, P. Tristant, J. Desmaison, P. Leprince, Spectrochimica Acta Part B: Atomic Spectroscopy, vol. 61, no. 1, pp. 2-30, 2006; https://doi.org/10.1016/j.sab.2005.10.003
[29] Q. Zhang, C. Li, Nanomaterials, vol. 8, no. 10, p. 827, 2018; https://www.mdpi.com/2079-4991/8/10/827.
[30] B. Sankapal, M. C. Lux-Steiner, A. Ennaoui, Applied surface science, vol. 239, no. 2, pp. 165-170, 2005; https://doi.org/10.1016/j.apsusc.2004.05.142
[31] O.-G. Simionescu, C. Romaniţan, O. Tutunaru, V. Ion, O. Buiu, A. Avram, Coatings, vol. 9, no. 7, p. 442, 2019; https://www.mdpi.com/2079-6412/9/7/442.
[32] A. A. Haidry et al., Key Engineering Materials, vol. 510-511, pp. 467-474, 2012,; www.scientific.net/KEM.510-511.467.
[33] J.-Y. Zheng, S.-H. Bao, Y. Guo, P. Jin, ACS Applied Materials & Interfaces, vol. 6, no. 3, pp. 1351-1355, 2014; https://doi.org/10.1021/am404470e
[34] M. Procek, A. Stolarczyk, T. Pustelny, E. Maciak, Sensors, vol. 15, no. 4, pp. 9563-9581, 2015; https://doi.org/10.3390/s150409563
[35] S. Agarwal, Y. Prajapati, J. Maurya, IEEE Photonics Technology Letters, vol. 28, no. 21, pp. 2415-2418, 2016; https://doi.org/10.1109/LPT.2016.2597856
[36] O. V. Sizova, N. V. Teryukalova, A. A. Leonov, Y. A. Denisova, O. S. Novitskaya, A. V. Kolubaev, Russian Physics Journal, vol. 65, no. 7, pp. 1123-1129, 2022/11/01 2022; https://doi.org/10.1007/s11182-022-02740-z
[37] M. S. Farhan, Wasit Journal of Engineering Sciences, vol. 4, no. 1, 2016.
[38] S. Yang, G. Lei, H. Xu, Z. Lan, Z. Wang, H. Gu, Nanomaterials, vol. 11, no. 4, p. 1026, 2021; https://www.mdpi.com/2079-4991/11/4/1026.
[39] S. Jayawardena, H. D. Siriwardena, R. M. G. Rajapakse, A. Kubono, M. Shimomura, Applied Surface Science, vol. 493, pp. 250-260, 2019/11/01/ 2019; https://doi.org/10.1016/j.apsusc.2019.06.280.

[40] K. Tang, X. Chen, X. Ding, X. Yu, X. Yu, ACS Applied Nano Materials, vol. 4, no. 10, pp. 10810-10818, 2021/10/22 2021; https://doi.org/10.1021/acsanm.1c02249
[41] S. Banerjee, E. Adhikari, P. Sapkota, A. Sebastian, S. Ptasinska, Materials, vol. 13, no. 13, p. 2931, 2020; https://www.mdpi.com/1996-1944/13/13/2931.
[42] H. Fakhouri, D. B. Salem, O. Carton, J. Pulpytel, F. Arefi-Khonsari, Journal of Physics D: Applied Physics, vol. 47, no. 26, p. 265301, 2014/06/05 2014; https://doi.org/10.1088/0022-3727/47/26/265301
[43] J. Kankare, Langmuir, vol. 18, no. 18, pp. 7092-7094, 2002; https://doi.org/10.1021/la025911w
[44] X. Wang, F. Cui, J. Lin, B. Ding, J. Yu, S. S. Al-Deyab, Sensors and Actuators B: Chemical, vol. 171-172, pp. 658-665, 2012/08/01/ 2012; https://doi.org/10.1016/j.snb.2012.05.050.
[45] Y.-C. Lin, M.-J. Wang, Japanese Journal of Applied Physics, vol. 58, no. SA, p. SAAC01, 2018/11/23 2019; https://doi.org/10.7567/1347-4065/aaea6c
[46] S. Zanini, E. Grimoldi, C. Riccardi, Materials Chemistry and Physics, vol. 138, no. 2, pp. 850-855, 2013/03/15/ 2013; https://doi.org/10.1016/j.matchemphys.2012.12.070.
[47] J. Li, Q. Yuan, X. Chang, Y. Wang, G. Yin, C. Dong, Plasma Science and Technology, vol. 19, no. 4, p. 045505, 2017/03/09 2017; https://doi.org/10.1088/2058-6272/aa57e4
[48] K. Dallah, A. Bellel, O. Lezzar, S. Sahli, P. Raynaud, Key Engineering Materials, vol. 826, pp. 67-72, 2019; https://doi.org/10.4028/www.scientific.net/KEM.826.67
[49] K. a. B. Dallah, A. and Lezzar, O. C. and Sahli, S., Digest Journal of Nanomaterials and Biostructures, vol. 18(1), pp. 279–290, (2023); https://doi.org/10.15251/DJNB.2023.181.279
[50] M. Nakamura, D. Korzec, T. Aoki, J. Engemann, Y. Hatanaka, Applied Surface Science, vol. 175-176, pp. 697-702, 2001/05/15/ 2001; https://doi.org/10.1016/S0169-4332(01)00140-4.
[51] S. Jayawardena, A. Kubono, R. M. G. Rajapakse, M. Shimomura, Nano-Structures & Nano-Objects, vol. 28, p. 100780, 2021/10/01/ 2021; https://doi.org/10.1016/j.nanoso.2021.100780.
[52] C. Piferi et al., Nanomaterials, vol. 12, no. 3, p. 533, 2022; https://www.mdpi.com/2079-4991/12/3/533.
[53] G. Jnido, G. Ohms, W. Viöl, Coatings, vol. 9, no. 7, p. 441, 2019; https://www.mdpi.com/2079-6412/9/7/441.
[54] M. J. Uddin et al., Frontiers in Materials, vol. 7, p. 192, 2020
[55] L. Ghazaryan et al., Nanotechnology, vol. 32, no. 9, p. 095709, 2020/12/10 2021; https://doi.org/10.1088/1361-6528/abcbc1
[56] A. Uricchio, F. Fanelli, Processes, vol. 9, no. 11, p. 2069, 2021; https://www.mdpi.com/2227-9717/9/11/2069.
[57] W. Zeng, T. Liu, Z. Wang, Physica E: Low-dimensional Systems and Nanostructures, vol. 43, no. 2, pp. 633-638, 2010/12/01/ 2010; https://doi.org/10.1016/j.physe.2010.10.010.
[58] R. H. Rosa, Atividade fotocatalítica e antimicrobiana de filmes de TiO2: alternativa sustentável para autolimpeza de superfícies, Universidade de São Paulo, 2023.
[59] X. Li, Y. Zhao, X. Wang, J. Wang, A. M. Gaskov, S. A. Akbar, Sensors and Actuators B: Chemical, vol. 230, pp. 330-336, 2016/07/01/ 2016; https://doi.org/10.1016/j.snb.2016.02.069.
[60] Z. Ye et al., Materials Letters, vol. 165, pp. 127-130, 2016/02/15/ 2016; https://doi.org/10.1016/j.matlet.2015.11.129.
[61] A. Esfandiar, S. Ghasemi, A. Irajizad, O. Akhavan, M. R. Gholami, International Journal of Hydrogen Energy, vol. 37, no. 20, pp. 15423-15432, 2012/10/01/ 2012; https://doi.org/10.1016/j.ijhydene.2012.08.011.
[62] M. Boutamine, A. Bellel, S. Sahli, Y. Segui, P. Raynaud, Thin Solid Films, vol. 552, pp. 196-203, 2014/02/03/ 2014; https://doi.org/10.1016/j.tsf.2013.12.016
[63] H. Peng et al., Molecules, vol. 29, no. 7, Apr 7 2024; https://doi.org/10.3390/molecules29071657
[64] V. O. Vo, T. L. Pham, V. A. Dinh, Materials Transactions, vol. 61, no. 8, pp. 1449-1454, 2020; https://doi.org/10.2320/matertrans.MT-MN2019022
[65 T. Cowen, M. Cheffena, International Journal of Molecular Sciences, vol. 23, no. 17; https://doi.org/10.3390/ijms23179642

[66] L. Grine, A. Bellel, M. Boutamine, S. Sahli, Proceedings of the 2nd International Conference of Nanotechnology for Environmental Protection and Clean Energy Production, Singapore, S. Hamamda, A. Zahaf, Y. Sementsov, S. Nedilko, and K. Ivanenko, Eds., 2024// 2024: Springer Nature Singapore, pp. 217-224.
[67] D. Zhang, H. Chang, P. Li, R. Liu, Q. Xue, Sensors and Actuators B: Chemical, vol. 225, pp. 233-240, 2016; https://doi.org/10.1016/j.snb.2015.11.024